SunChase: Energy-Efficient Route Planning for Solar-Powered EVs

Landu Jiang*, Yu Hua†, Chen Ma* and Xue Liu*
*School of Computer Science, McGill University, Montreal, Quebec, Canada
†WNLO, School of Computer, Huazhong University of Science and Technology
Wuhan, China

Abstract—**Electric vehicles (EVs) play a significant role in the current transportation systems. The main factor that affects the acceptance of existing EV models is the range anxiety problem caused by limited charging stations and long recharge times. Recently, the solar-powered EV has drawn many attentions due to being free of charging limitations. However, the solar-powered EVs may still struggle with the limited use because of unpredictable solar availability. For example, shadings caused by buildings and trees also possibly decrease the solar panel cell efficiency. To address this, we propose a route planning method for solar-powered EVs to balance the energy harvesting and consumption subject to time constraint. The idea behind our solution is to offer power-aware optimal routing, which maximizes the on-road energy input given solar availability on each road segment. We first build a solar access estimation model using 3D geographic data and then employ a multi-criteria search method to generate a set of Pareto candidate routes. In order to reduce the size of the set, we leverage the bisect k-means clustering algorithm to extract the most representative Pareto routes with better solar availability. In the evaluation, we developed a validation platform on the vehicle and leveraged mobile sensing techniques to examine our proposed model in real road environments. We conducted simulations to evaluate our proposed route planning algorithm using real life scenarios. Experimental results demonstrate that our solar input model is robust to real road scenarios, and the routing algorithm has great potential to provide efficient services for solar-powered EV in the future.**

Index Terms—**Route Planning, Solar Power, Electric Vehicle.**

I. INTRODUCTION

The market share of Electric vehicle (EV) has significantly increased over the past few years, which is considered as one of the most promising transportation tools of the future. In 2015, there has been over 1 million EVs on the road, and a 20% steady increase of annual growth rate of the global EV market is predicted before 2020. Compared with gasoline-powered vehicles, EVs take advantages of the ability to obtain electricity from a broad range of regenerative energy sources, such as tidal power, solar power and wind power. However, electric vehicles on the market today still face several challenges despite the wide acceptance. Small battery capacity and sparse availability of charging stations are considered to be major factors that limit the range of EVs, which is so-called the range anxiety problem [1], [2]. Though a number of charging facilities have been designed and installed such as home charging point and workplace charging facility [11] [24]. These charging facilities may increase the infrastructure cost and hour-scale recharge time is not able to meet the consumer demand.

Due to the flexibility to integrate different energy generators, EVs can power accessories (e.g., light and audio system), fuel the battery or direct the energy straight to the electric motor partly or totally relying on solar energy [3]. As a special class of EV models, the solar-powered EV has been considered as a solution to the range anxiety problem and drawn many attentions from both academia and industry. Solar-powered EVs use the solar panels installed on the car to collect energy, which can convert the solar energy into electricity not only at parking but also travelling on the road. Although successfully being freed from charging limitations (e.g., limited charging resources, long charging time), the solar-powered EV may still struggle with inefficient energy input due to unpredictable solar availability. Especially in urban areas, solar-powered EVs can hardly harness enough solar energy due to intermittent shadings caused by buildings and road-side trees. Several routing algorithms have been proposed to solve the range anxiety problem for ordinary EVs [4], [5]. They aim to minimized the EV energy cost for a given trip by selecting an optimal route. However, the problem of route optimization for a solar-powered EV is even more challenging due to solar access variations as well as time constraints. A previous study [1] seeks to optimally plan the speed for solar-powered EVs on different road segments (i.e., illuminated road and shaded road) to balance energy harvesting and consumption, which enables the driver to reach the destination in the shortest time. Unfortunately, authors do not consider the EV route planning problem with real urban street restrictions. Different routes have different lengths, levels of congestion and solar availability, all of which would significantly affect the vehicle speed, fuel consumption and solar energy input efficiency. The system should be able to select a route for the driver that maximize the solar power collection with less extra energy/time costs.

Moving along this direction, in this paper we propose a route planning algorithm for solar-powered EVs, which aims to help the driver to complete a given trip in urban areas with maximal solar availability. The basic idea of our approach is to define the route planning as a multi-objective optimization problem that incorporates three major factors including travel time, solar-input/access quantity and EV energy consumption. By integrating the solar access model and traffic flow information,

IEEE computer society

we employ a multi-criteria search algorithm to find a set of Pareto routes between two locations. Finally, we could offer better routing plans to drivers based on different personal preferences/demands (e.g., travel time, EV model type).

To implement the proposed route planning algorithm, we addressed several challenges in practice. Firstly, there might be a large number of Pareto routes generated by the multi-criteria algorithm. While we only need a small set of candidate routes (e.g., 2-3 routes). The comparison between each pair of routes is time consuming and many of them have similar properties (e.g., 90% nodes and edges). Secondly, due to efficiency limitations, an EV may deplete the energy faster than the solar input. We need to verify that the selected route can produce more energy input than the consumption on extra travel distance compared to shortest-time path. Thirdly, urban solar input/access estimation is a challenging task. Since the on-road solar input information is not accessible via any public database. A large-scale solar radiation sensing network is not affordable [6]. Finally, there is no solar-powered EV model on the market. The evaluation of the solar input model and our proposed route planning algorithm is not an easy task.

Specifically, we make the following contributions:

1) We proposed a multi-criteria route optimization algorithm for the solar-powered EV, which considers travel time, solar access availability and EV energy consumption. We propose a novel route merging method, which leverages the bisect k-means clustering algorithm to extract the most representative Pareto routes. We also define the candidate route selection scheme to determine the driving path.

2) In order to build daytime solar access model, we use the ArcGIS 3D scene tools to capture local (City of Montreal) shading scenes while at the same time using computer vision algorithms to measure solar availability on roads. By integrating the solar access data and traffic flow information, we are able to estimate the solar energy input on each road segment.

3) We conduct real-road driving experiments and simulations to evaluate our proposed method. We also developed a solar perception prototype to validate the solar input map estimation on real-road driving. We studied two driving scenarios in the simulation to examine the routing performance of our proposed algorithm. Experimental results show that our solar input estimation model, as well as the route planning algorithm are robust to real road scenarios, and has great potential to provide desirable services for solar-powered EV in the future.

Additionally, we do not consider the speed planning problem for solar-powered EVs in our design. It has been well studied by Lv's work [1]. In case where it is required, two works can be integrated to achieve the goal. We also acknowledge that existing ordinary EVs are not equipped with solar panels. In addition, the energy consumption of EV is much higher than solar energy input due to cell limitations especially in high speed modes. However, the purpose of our solution is to provide driving routes with better solar availability to drivers,

the EV can arrive the destination in time while receive the extra energy input. It could be more useful in the future on new solar-powered EVs where solar panels serve as the main or minor energy input.

The reminder of the paper is organized as follows. Section II reviews the related work. Section III gives a brief view of the problem considerations and the algorithm design. Section IV presents the proposed route planning algorithm and our solar access model. Section V presents real driving experiments and simulation results. Section VI discusses the future work to improve the system performance and Section VII concludes the paper.

II. RELATED WORK

There has been active research work addressing electric vehicles (EVs) path planning problems with the objective of minimizing energy consumption. Most of the path planning problems can be summarized into the Constrained Shortest Path (CPS) category [7]. Several approaches have been proposed to address EV routing problem [8], [9], [10], which are subject to trip constraints such as travel time, energy capacity and charging station distribution, etc.. However, their solutions do not consider the solar energy input during the trip. In addition, some research work also focuses on the energy recuperation scenario, Artmeier et al. [11] studied optimal routing for electrical vehicles with rechargeable batteries within a graph-theoretic context. They formalized the routing problem as a special case of the constrained shortest path problem (CSP) with several hard and soft constraints and used a family of search algorithms to address these constraints. To further speedup the performance of algorithm for path planning problem with recuperation, Baum et al. [12] presented a dynamic method for Customizable Routing Problem (CRP), which is capable of updating the energy matrix in real time as the vehicles storage solar energy during trip. The recuperation process in their models is similar to the solar energy input on illuminated roads, which could resemble and inspire our design. The major difference between our work and these research is that the energy collected via recuperation is assumed to be a fixed value on each road segment, while the solar energy input value is affected by travel time and solar radiation.

On the other hand, the studies of maximizing solar energy harvest in UAVs (Unmanned Arial Vehicles) path planning problem [13], [14], [15] have emerged in the last decade. The mathematical models are targeted at aircrafts instead of automobiles, and so their dynamics include back angle control variable which is different from vehicle models. Take a glance at the competition of solar-powered EV design, the models presented by the competitors in the American Solar Challenge [16] mainly focus on optimizing the EV shape to decrease the wind drag, as well as expanding the effective area of solar panels to maximize energy input. Nevertheless, the EV routing problem are not considered in the competition.

Towards the most related work in solar-powered EVs path planning problem, Plonski et al. [17] addressed the minimal-

energy path planning problem for solar-powered mobile robots. The authors estimate the overall solar distribution of a certain bounded testing area based on the sampling data of certain points, and calculate the minimal energy consumption path using the estimates in solar map. However, the path planning model can be less practical if one considers the change of shadows as the sun moves in the sky, or extends the robots to automobile and takes the numerous and complex urban streets constraints into consideration. Sorrentino et al. [18] presented a genetic algorithm to calculate the path with minimal fuel consumption for hybrid solar vehicles. The solar energy are collected from a stationary photovoltaic plant, which did not consider shaded road segments in the course of data requisition. Moreover, Lv et al. [1] proposed a dynamic programming method to compute the optimal speed assignment on each path segment to minimize the total travel time. The computation overhead is notably decreased compared with standard non-linear programming solver and the estimates are proved to be fit well with the real data from physical EV. However, their solution is built upon speed planning. A driver can not select an optimal path to maximize the solar energy collection. In our design, we aim to find the most energy-wise path with optimal tradeoff between the solar energy input and the additional energy cost for the trip.

III. DESIGN CONSIDERATIONS

In this section, we discuss the technical considerations underpin the design of solar-powered EV routing while the detailed algorithm design is presented in Section IV.
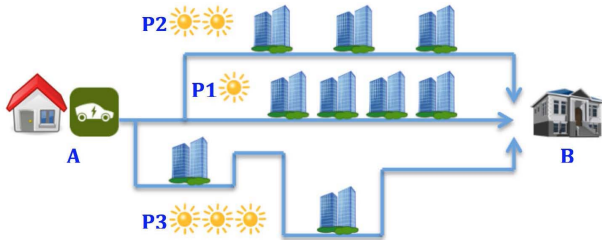

Fig. 1: The Solar-Powered EV Routing Problem

A. The Route Planning Problem

The route planning problem can be explained using the example as shown in Figure 1. When a user starts a trip from home A to the workplace/school B. There will be three types of path options, $P1$ the shortest-time path but little solar energy input, $P2$ a little longer travel time with higher solar energy input and $P3$ maximal solar energy input in an acceptable arrival time. In this work, we assume that the vehicle speed is constant on each road segment, the travel time mainly depends on the traffic flow and the route length.

If the driver is late for work/class and the arrival time is the first priority, he/she drives a gasoline or ordinary battery-powered electric vehicle. Without considering traffic situation, the shortest path $P1$ would be the best option. However, $P1$

has many shaded road segments caused by buildings and trees, which has limited solar energy input. If the vehicle battery totally relies on the solar power, it may not have enough energy to reach the destination. Comparably, other longer paths ($P2$ and $P3$) are more feasible if the driver have enough time. Moreover, since many paths have similar length (e.g., no more than 100 meters) in urban areas, the energy cost on $P2$ could be very close to $P1$. Then $P2$ is a better choice than $P1$ if the user drives a solar-powered EV which requires more solar energy input.

B. Multi-Criteria Routing Path Model

In this paper, the vehicle route network can be represented as a directed weighted graph $G = (V, E, \mathbf{c})$, where V is the set of nodes, and each node on the map corresponds to an intersection with geographic coordinates (i.e., latitude and longitude). The edge set $E = (u, v)|(u, v \in V) \wedge (u \neq v)$ represents the road segments on real roads that connect two intersection nodes. An example of road segments in a path is shown in Figure 2, given a start point A and an end point B, the path from A to B is composed of consecutive road segments (edges) that can be defined as follows:

$$P(A, B) = < S_{start}, S_1, S_2, ...S_n, S_{end} > \qquad (1)$$

where S_{start} and S_{end} are the road segments from start the point A and the end point B to their nearest neighbour intersections (I_1 and I_3), and $S_i (i = 1, 2, ..., n)$ are road segments (edges) that between connected intersections (nodes). In addition, one road segment may also be composed of several illuminated segments and shaded segments. But we do not further divide a single road segment into smaller segments (illuminated/shaded segments), because a driver can not change the path between two neighbour intersection nodes (e.g., I_1 and I_2 in Figure 2).
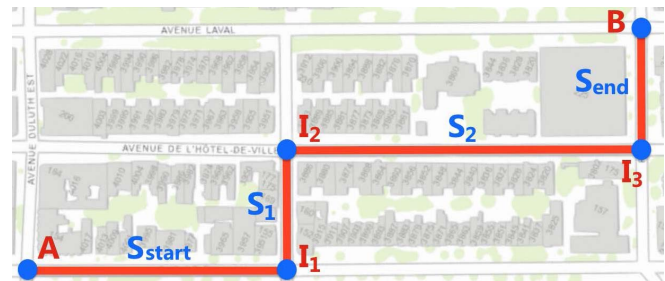

Fig. 2: An Example of the Path from A to B, I_1 is the neighbour intersection to A and I_3 is the neighbour intersection to B.

As we consider the EV route planning as a multi-criteria problem, the cost on each edge is represented as a k-dimensional vector of criteria $\mathbf{c} = (c_{tt}, c_{si}, ..., c_k)$. Since we have two attributes to be taken into consideration, i.e., road distance and solar-input, we define $k = 3$. The solution of the multi-criteria vehicle routing problem is a full Pareto set of routes π, each route in this set with a vector of cost value $c(\pi_p)$ is non-dominated by any other solutions (a solution π_p dominates

another solution π_q iff $c_i(\pi_p) \leq c_i(\pi_q)$ for all $1 \leq i \leq k$, and $c_j(\pi_p) < c_j(\pi_q)$, for at least one j, $1 \leq j \leq k$).

C. Solar Access Model

1) Solar Road Segments: In this paper, we compute the route planning for solar-powered EVs in urban areas, where shadows cast by trees and buildings can limit the solar input/access on road. Since each road (edge) consists of illuminated segments and shaded segments [1]. We consider EVs equipped with solar panels which can only collect solar energy on illuminated/solar road segments (e.g., during the trip or at the parking lot). Extracting the information of solar road segments from existing public databases (e.g. ArcGIS[3], Google Maps) is a challenging task.

2) Solar Travel Time: Nowadays, different types of solar panel products could have different cell efficiency [1], and it is difficult to build a standard solar energy map for all solar-powered EVs due to lack of industrial information and solar-powered EV. According to [1], on an illuminated road segment with length S_{Solar} with a constant cruising speed V, the actual power output of a solar panel is a fraction of the total solar power, which can be expressed by Equation 2,

$$Energy_{Solar} = C \cdot \frac{S_{Solar}}{V}, \tag{2}$$

where C is the power input of solar panel on illuminated segments. In this paper, we assume C is constant in short trips and there will be a value update every 15 minutes (discussed in Section IV-B). We estimate the solar power input C based on the average cell efficiency of commercial solar panel products (around 20%) [1]. Therefore, the solar-energy availability of each path only relies on the length of illuminated road segments S_{Solar} and the vehicle speed V, which can be expressed as the EV travel time on solar road segments t_{Solar} (Equation 3).

$$t_{Solar} = \frac{S_{Solar}}{V}, \tag{3}$$

In this paper, t_{Solar} is called solar travel time. We measure the t_{Solar} instead of validating the solar energy input value on candidate driving paths to select proper routes for solar-powered EVs.

3) Solar Road Length and Radiation: Given a road segment edge e_n ($1 < n < m$) in the path, the road length s_n is the sum of illuminated length s_n^{Solar} and shaded length s_n^{Shadow}. The illuminated road length S_{Solar} of the entire path can be expressed by Equation IV-B2,

$$S_{Solar} = \sum_{n=1}^{m} s_n^{Solar}. \tag{4}$$

The value of solar length s^{Solar} can be measured by subtracting the shading segments s^{Shadow} from the road. Shading segments that casted by buildings/trees can be predicted/estimated by applying the ray-tracing technique (e.g., ArcGIS [3] tools) given the current time (to compute solar path and position) and building/tree information (e.g., height, size, location). However,

shading segments on roads fails to (or very less likely) obtain regular shapes and change significantly throughout a day. It is because that shadows rotate around the objects (e.g. buildings and trees) that cast them during the daytime along with different sun's positions (Earth rotates). For example, the shadow casted by one high building at an intersection may cover two or three roads in the morning and dim one entire street in the afternoon.

What is more, the amount of solar radiation incident on the EV's flat panel changes with the position of the sun (i.e.elevation angle). The selected paths have different solar energy accesses at different times of the day. Figure 4 shows an example of the daily value of the local solar radiation. We observe that the solar radiation value is low in the morning and evening while reaches the highest level at noon. Therefore, estimating solar access is a very challenging task which may require a large-scale radiation sensing network on urban roads. In this paper, we propose a vision-based solution to measure street-level solar input/access. The detailed description of the algorithm is presented in IV-B.

D. Solar-Oriented Routing

A longer driving path will deplete more vehicle energy. The routing algorithm for solar-powered EVs should be able to manage the balance between the EV energy consumption and solar energy input (as shown by Equation 5). Compare with the shortest path P_1, a driver has to collect enough solar energy for extra energy cost on path P_i,

$$\begin{aligned} Energy_i^{Extra} &= (Energy_i^{Solar} - Energy_1^{Solar}) \\ &- (Energy_i^{Out} - Energy_1^{Out}) > 0, \end{aligned} \tag{5}$$

in Lv's work [1], the energy consumption of EV E_{Out}^i on path P_i can be expressed by Equation 6.

$$Energy_{Out} = S(aV^2 + b), \tag{6}$$

where parameters a and b are determined by the vehicle itself and the road conditions. Thus, based on Equations 5, 2 and 6, we can select the best path from candidate routes that meets the requirements.

Therefore, the intuitions and experience in planning trip for traditional combustion engine vehicles and ordinary battery-powered electric vehicle fail to be used for solar-powered EVs. The situation could become even more complex due to various solar availability during the daytime. In order to make the driver successfully complete the trip and meet timing requirements, the route of the trip must be systematically planned according to complex road situations and solar input/access conditions. So in this paper, we study the travel route planning which enables the solar-powered EV to collect more energy input within acceptable travel time.

IV. SOLAR-ORIENTED ROUTE PLANNING ALGORITHM

In this section, we present how to generate the properties of the routes. There are three criteria taken into account, i.e., the route distance and the solar-input. Then we illustrate how

to address the multi-criteria routing problem via the multi-label correcting algorithm. At last, a set of Pareto routes are displayed and the optimal route is selected from the Pareto set.

A. Road-Segment Distance Calculation

As mentioned in Section III-B, we represent the vehicle road network as a directed weighted graph. Each edge $(u, v) \in E$ in the graph represents a road segment. Since each node has a geographic coordinate, thus we apply Haversine formula to calculate the geographic length of a road segment [19]. Eq. 7 displays how to use the latitude and longitude to compute the distance between two nodes,

$$
\begin{aligned}
d = & 2r \ arcsin(\sqrt{A + B}), A = sin^2(\frac{\varphi_2 - \varphi_1}{2}), \\
& B = cos(\varphi_1)cos(\varphi_2)sin^2(\frac{\lambda_2 - \lambda_1}{2}),
\end{aligned} \tag{7}
$$

where φ_1 and φ_2 are the latitude and longitude of node u, λ_1 and λ_2 are the latitude and longitude of node v, r is the radius of the sphere. We use this equation to obtain the distance of all edges.

B. On-Road Solar Input Modeling

1) Solar Input Map: Instead of deploying a large-scale solar radiation sensing network [6], we present an efficient method using vision-based techniques to estimate the solar access on urban roads. The basic idea of our method is to build a solar input map by measuring the length of shaded and illuminated areas of each road segment based on ArcGIS 3D local scenes [20] and solar radiation datasets [21]. 3D scene in ArcGIS is the primary framework for geo-information modeling. It contains the building layer (3D modeling) and sunlight/daylight features, which allows us to generate on-road shadows by integrating and combining the 2D basemap.

We first select the 3D scene of the city (Montreal) and use the time as the input to simulate the sunlight conditions in ArcGIS. We then take the 2D imagery (map) (top-down view) of 3D scenes (Figure 3) and analyze shaded/illuminated road segments in the map using vision-based methods. Based on the shadow information extracted from 3D scenes, we are able to estimate the solar access of different paths on real roads and help drivers to select proper routes for their solar-powered EVs. In addition, shadows rotate around objects (e.g., buildings) due to different positions of the sun (Section III-C). As shown in Figure 3a and 3b, shaded regions in 3D scenes have different shapes at different times (at 9:15 a.m. and 3:15 p.m.). To collect daytime shadow data we take 3D scene images throughout one consistently sunny day (from 8:00 a.m. to 6:30 p.m. in the test). According to our real-road test and solar radiation data [21], we choose 15 minutes as the sampling interval of the imagery data, which could draw a balance between the computation workload and the estimation quality of our planned paths (shaded road segments do not change significantly).

2) Solar Road Length Estimation: Measuring the length of shadows for a given road segment S_i in 3D scenes is very challenging (It is hard to select endpoints.). Instead, we first calculate the area ratio r_{area} of shaded parts A_i^{Shaded} to the target road segment A_i in selected images. Based on the basic geometry, the road area ratio is very close to the road length ratio if the road width does not change significantly. Thus, the road area ratio (A_i^{Shaded} to A_i) in the image can be considered as an approximation to the length ratio r_{length} of shaded segments L_i^{Shaded} to the target road segment L_i. We then calculate the shaded road length L_i^{Shaded} based on the area ratio r_{area} in 3D scenes and the road length L_i (L_i is measured based on the real location information), which indicates the probability of solar loss when we drive through the road segment S_i as follows:

$$
r_{area} = \frac{A_i^{Shaded}}{A_i} \approx r_{length} = \frac{L_i^{Shaded}}{L_i}, \tag{8}
$$

$$
L_i^{Shaded} \approx L_i \cdot r_{area}, \tag{9}
$$

To measure the area of a road segment in the image, we employ the binarization method to extract the road region and calculate the amount of pixels in it. We then leverage a Probabilistic Hough-line transformation to identify the line segment for each road and locate intersection points/nodes in the map. Based on the geographic information in the graph G, we are able to build the solar map with nodes corresponding to real physical intersections on road and assign the value (length and area) to each road segment/edge in the model. Finally, the illuminated segment length of each road can be estimated using the solar map. In addition, the Hough-line transformation may not be able to achieve 100% accuracy, we also manually add and correct intersection points/nodes on images.

3) Solar Radiation and Traffic Flow: Given one road segment S_i with a fixed solar length L_i^{Solar} (constant in 15 minutes), the amount of solar energy that a EV can collect relies on the travel time t_i^{Solar} and current solar irradiance P_t. In urban areas, the vehicle speed V_i is largely affected by the traffic low. Since we do not consider the speed planning problem in this paper, we choose the EV speed based on the traffic flow information provided by Google Maps [22]. Thus, we can estimate the EV travel time t_i^{Solar} on a selected solar road segment using the current traffic speed and the solar road length produced by the last Section IV-B2.

To obtain the solar irradiance information, we make use of the solar radiation datasets which were retrieved from a system composed of 17 units (each unit has two irradiance sensors) at one of Canadian sites located in Quebec (very close to Montreal). The system measured the ground-level solar variability on a network of sensors distributed over a given surface. The measurement was performed at a high frequency (up to once every 10 milliseconds), which can record high ramp-rate events and help simulate the solar radiation in urban areas. Figure 4 shows the solar radiation data for a day in July, we can see that the solar irradiance achieves maximum value (around 1150 W/m^2) in the middle of the day and become

(a) On-road Shading (9:15 AM).   (b) On-road Shading (3:15 PM).

Fig. 3: Examples of Shading Segments on Urban roads.

lower in the early morning and evening (less than 300 W/m^2). The solar radiation data is from Natural Resources Canada [21]. The surges in the measured irradiance on a unit were mainly caused by obstructions (e.g., birds) passing over or variable cloud cover conditions.
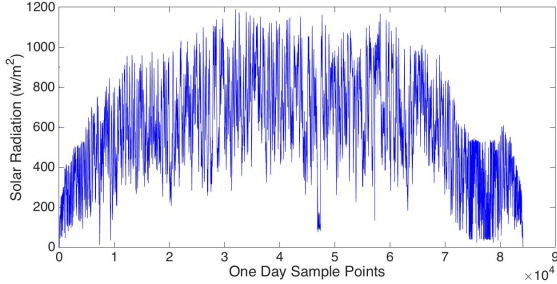

Fig. 4: An Example of Solar Radiation Value for One Day in Quebec.

C. Multi-label Correcting Algorithm

In this paper, we use the multi-label correcting algorithm to compute the full set of Pareto routes [23], which operates on labels that have multiple values, one per optimization criterion. To execute the algorithm, we define variable structures for each node $u \in V$, label $L(u) := (u, (l_{tt}(u), l_{si}(u), ..., l_k(u)), L^P(u))$, which is composed of the node cost values with respect to each criterion, and the label $L^P(u)$ represents L(u)'s predecessor. We define k = 3 in our route planning algorithm, where l_{tt}, l_{si} and l_{ec} represents the travel time, solar energy input and EV energy consumption, respectively. In addition, each label has a sequence number starting from 0. A priority queue $Queue_L$ is created to store all labels built during the search. Since each node may be searched multiple times, we define a *set* structure $BagofLabel(u)$ for each node to maintain the non-dominated labels at u.

The main steps of multi-label correcting algorithm (pseudocode of Algorithm 1) are shown as follows:

(1) For a three-criterion optimization problem, we first do the initialization,

---

Algorithm 1: Multi-Criteria Routing Algorithm

Input: vehicle route graph $G = (V, E, \mathbf{c})$, origin node s, target node t
Output: full Pareto routes set $P(t)$
Initialization:
Initialize the label of origin node L(s) ;
Q.add(L(s)) ;
P(s).add(L(s)) ;
while *Q is not empty* **do**
  current := Q.pop_min() ;
  u := getNode(current) ;
  $(l_{tt}(u), l_{si}(u), l_{ec}(u))$:= getCost(current) ;
  $L^P(u)$ = getPredecessorLabel(current) ;
  foreach *edge* (u, v) **do**
    | to_insert := ComputeNewCosts()
  end
  foreach *Label* $L(v) \in P(v)$ **do**
    | to_insert := CheckDomination()
  end
  if *to_insert == True* **then**
    next := $(v, (C_{tt}(v), C_{si}(v), C_{ec}(v)), L_{current})$;
    P(v).add(next) ;
    Q.add(next) ;
  end
end

- we initialize the label at the start point $L(origin) := (u_o, (0, 0, 0), preL(origin))$, where preL(origin) is NULL;
- insert the initial label $L(origin)$ into $Queue_L$ and $BagofLabel(origin)$.

(2) Secondly, we need to extract the minimum label (in lexicographic order) at current step $L_{current}$ from the priority queue $Queue_L$. For each edge (u, v) out of node u:

a. Compute new cost values $c_{tt}(v), c_{si}(v), c_{ec}(v)$ from u to node v. Specifically, unlike other EV energy saving cases, we expect the maximum value of solar energy input. We compute the $c_{si}(v)$ by calculating the EV travel time on shaded road segments. Since less shadows means more solar input.

b. If the new cost values are not dominated by any label $L(v) \in BagofLabel(v)$, create a new label $(v, (c_{tt}(v), c_{si}(v), c_{ec}(v)), L_{current})$ for node v and then insert this new label into $Queue_L$ and $BagofLabel(v)$.

c. If any label $L(v) \in BagofLabel(v)$ is dominated by the new cost values $(c_{tt}(v), c_{si}(v), c_{ec}(v))$, remove the label from the priority queue $Queue_L$ and $BagofLabel(v)$.

(3) Finally, if the priority queue $Queue_L$ becomes empty, exit the loop; otherwise, go to (2) and continue.

D. Optimal Route Selection

The multi-label correcting algorithm may generate a large set of Pareto routes, many of which may have the same properties and do not interest the users. We therefore need a method to select a small representative subset of Pareto routes. We

employ the bisect k-means clustering algorithm on the whole Pareto routes set to automatically decide the number of clusters. The Manhattan distance is used as the distance measure.

The bisect k-means algorithm works as follows. Initially, there is only one cluster which contains all the routes. The algorithm iteratively picks one cluster with the worst quality, then splits this cluster into two clusters. In our case, the cluster quality of a cluster $C = route_label1, ..., route_labeln$ is defined as $q(C) = \frac{1}{n} \sum_{i=1}^{n} |\mathbf{route\_label_i} - \mathbf{c}|$ where $\mathbf{c}$ is the centroid of C, i.e., $\frac{1}{n} \sum_{i=1}^{n} \mathbf{route\_label_i}$. A smaller $q(C)$ indicates better cluster quality. The algorithm terminates when $\forall C : [q(C) < \delta]$ where δ is predefined threshold for the cluster quality.

After route clustering, we need to select a small number of representative routes from these clusters. Route selection proceeds in two steps. In the first step, we select the so-called $single - cost optimum$ Pareto routes, i.e., routes that the lowest cost value for one of the three criteria. In the second step, we only consider the clusters that did not contain any of the single-cost optimum routes. For each of the remaining clusters, we select one route that is closest to its cluster centroid. Thus, at the end, we have at least one route (e.g., the shortest-time path) from each of the clusters. If there are more than one routes, we then calculate the extra travel time and energy input $Energy^{Extra}$ on each route compared to the the shortest-time path. The routes with the positive value of $Energy^{Extra}$ will be selected as the final outputs.

V. EVALUATION

In this section, we present our experiments as follows:

1) We developed a solar illumination perception platform (on a normal vehicle) to validate our on-road solar access estimation model in real driving environments.

2) We conducted simulations to compare the performance of our proposed method (multi-criteria route planning) and the shortest-path (shortest travel time) algorithm. We selected different start points and end points based on the real geographic information (i.e., OpenStreetMap and Google Maps).

To evaluate our solar input model in real-road driving situations, we conducted a validation platform on a petrol engine vehicle (there is no solar-powered EV in the market). Since it may be not safe/legal to add solar panels on a traditional vehicle, we focused on validating the travel time on solar road segments instead of measuring the solar energy input value. We developed a solar illumination perception system leveraging mobile sensing techniques. We employed smartphone light sensors to monitor solar illuminance and detect when a vehicle enters or exits an illuminated/solar area while at the same time using the GPS units (embedded in smartphones) to record the vehicle location information. In order to avoid system glitches and variances caused by different sensor view angles [24], we ran the sensing applications on two Android smartphones (Google Nexus 6) simultaneously and mounted them at different positions (windshield and sunroof) in the vehicle, as shown in

Figure 5. Each smartphone is equipped with a Quad-core 2.7 GHz Krait 450 CPU, 3GB RAM.

To validate the proposed route planning solution to be used on existing ordinary EVs, our simulations were conducted based on real geographic/traffic data and EV energy consumption data. We collected road properties and traffic information from OpenStreetMap [25] and Google Maps [22]. In addition, we used the solar-powered EV prototype built in Lv's work [1] and the Tesla Model S (85kWh) as the testing EV models which are discussed in Section V-B. We use the pair of nodes (i.e., the start point and the end point) ID as the algorithm inputs and performed our proposed route planning algorithm to output a set of Pareto routes. We compared the solar availability on each route with the results generated by the shortest-path (shortest travel time) algorithm. Both algorithms were implemented and run within Python on a CentOS 7 server which has the Intel i5 CPU and 8GB memory.

A. Real Road Solar Access

We carried out real-road experiments in July and August at different time of the day: in the morning 10:00 - 11:00, at noon 12:30 - 13:30 and in the afternoon 16:00 - 16:30. We select 6 urban driving paths in Downtown Montreal and ran the validation experiments on two sunny days and one mostly sunny day. The system can determine whether the vehicle was on an illuminated/solar road segment by checking the average value of two smartphone readings. Based on the testing data, we are able to calculate the travel time that a vehicle took on solar road segment of each path and validate our estimation model. The results are the average value of three experiments which are shown in Table I.

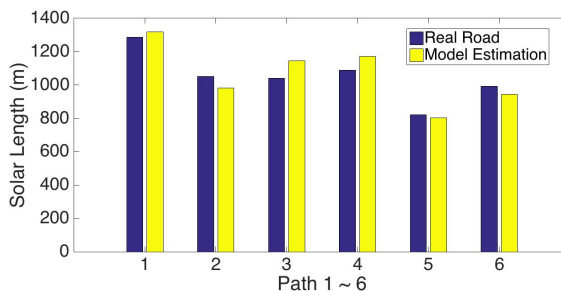Fig. 5: On-road Solar Access Experiment Setup.

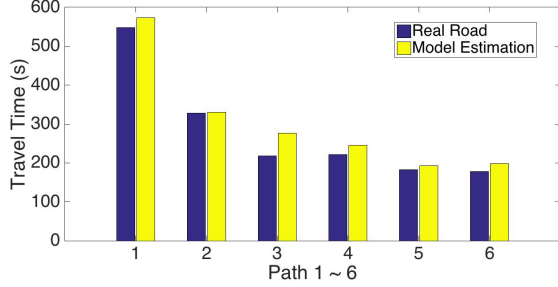Fig. 6: Real Road Solar Distance Validation.

389

Fig. 7: Real Road Travel Time Validation.

In Table I, RSD and MSD refer to the real road solar length and the solar length estimated by our model, RSTT and MSTT refer to the total travel time on solar road segments and the travel time estimated by our model, respectively. TS refers to the average speed of current traffic estimated by using Google Maps. Though there is slight difference in solar length and travel time between real driving and our estimation, the proposed solar input model can work well in real road environments.

For the solar length estimation, the differences are mainly caused by GPS errors on real road and the missing information in 3D scenes [20], since some roadside trees and other obstructions (may be temporarily built) that may cause shadows are not recorded in the database. For the travel time differences, a vehicle generally has different travel times on the same road segment. This is because a driver can not maintain a constant speed due to less accurate traffic flow prediction, different sensitivities of the acceleration pedal and personal driving style, etc.. For example, a driver may frequently drive faster than the average/predicted traffic speed, as we observe that in Table I the travel time in real test are all less than the estimation. Advanced automated and self-driving vehicles will be likely to perform stabilizing speed and follow the routing plan to collect proper solar energy.

To handle above issues, we may use mobile crowdsensing techniques to get the solar information from on-road vehicles and roadside units, which helps build a more accurate model and estimate real-time solar availability. The detailed plan is discussed in Section VI.

B. Solar Routing Simulation Results

In our simulations, we evaluated the proposed route planning algorithm using two real life scenarios: 1. Normal driving scenario; 2. One-day driving scenario. In the normal driving scenario, we analyze the solar energy input and travel time for driver one-way trips at different time of the day with different solar position and radiation. Since many people may need to drive all day such as food/mail delivery, Uber and Taxi services. We provide the one-day driving scenario to examine the amount of extra solar energy that a solar-powered EV can collect during the daytime.

We conducted the driving scenarios based on the real location data [25]. The length of each path generated in the simulations (for both scenarios) is 1 - 2.5 km, and the average vehicle speed on road segments is 14 - 17 km/h based on the traffic flow data. The solar radiation value will be updated every 15 minutes. To calculate the energy consumption, the parameters for the EV power output function is needed (e.g., a and b in Equation 6). According to Lv's tests [1], we set the precise values a = 0:01 and b = 33 for their solar-powered EV prototype. Since Tesla Model S is a much larger and heavier passenger car which aims to provide good road performance. Instead of using Lv's model, we estimate the energy consumption based on the official efficiency and range data [26].
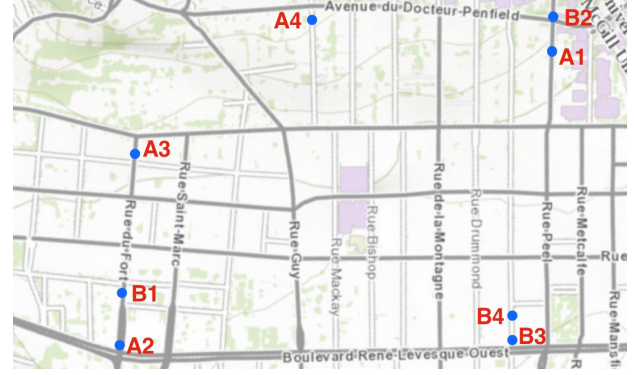

Fig. 8: Examples of Start and End Points for Real Road Experiments.

1) The Normal Driving Scenario: In the normal driving scenario, we present 3 driving cases with different solar radiations at different times of the day: case 1 (10:00 a.m.), case 2 (12:00 p.m.), and case 3 (4:00 p.m.), the solar inputs were set to 200W, 210W and 160W based on solar radiation datasets [21], respectively. We selected 4 different pairs of start and end points which correspond to real locations in the map, as shown in Figure 8.

Tables I, II, and III summarize the detailed results of route planning including the total road lengths (TL), total travel time (TT), total energy solar input (EI), total energy consumption of Lv's EV (EC1) and total energy consumption of Tesla Model S (EC2). In Table I, II, and III, we first show the shortest-time path from the start point A_i to the end point B_i, which is also one of candidate routes generated by our algorithm. Then we show other routes which achieved better extra energy input $Energy^{Extra}$, if there is no better route, we selected the shortest-time path as the routing result. The differences of energy input and consumption are listed in the tables. Since the multi-label correcting algorithm may output multiple candidate driving routes even after the optimal route selection (IV-D), we only present the most representative ones. The total number of candidate driving routes is listed in this table.

In Table II, the time is set to 10:00 in the morning. For A1-B1, we can not find any better route than the shortest-time path to get more solar input. But for A2-B2, which is nearly a reverse way of A1-B1 has two better routes. Since A2-B2 has a larger number of one-way road segments than A1-B1, which

TABLE I: Routing Simulation 10:00 AM

Paths	TL (m)	TT (s)	EI (Wh)	EC1 (Wh)	EC2 (Wh)
A1 to B1 3 candidate Pareto routes					
Shortest Time	1852	441.7	15.96	65.28	173.63
Better Solar	1852	441.7	15.96	65.28	173.63
A2 to B2 9 candidate Pareto routes					
Shortest Time	1992	474.3	16.51	70.22	186.75
Better Solar 1	1993	474.5	+0.97	+0.04	+0.09
Better Solar 2	2086	486.6	+6.41	+3.31	+8.81
A3 to B3 4 candidate Pareto routes					
Shortest Time	1624	386.7	13.70	57.25	152.25
Better Solar	1657	394.5	+1.34	+1.16	+3.09
A4 to B4 4 candidate Pareto routes					
Shortest Time	1433	341.2	10.21	50.51	134.34
Better Solar 1	1454	346.2	+4.08	+0.74	+1.97
Better Solar 2	1455	346.4	+5.92	+0.78	+2.06

TABLE II: Routing Simulation 12:00 PM

Paths	TL (m)	TT (s)	EI (Wh)	EC1 (Wh)	EC2 (Wh)
A1 to B1 3 candidate Pareto routes					
Shortest Time	1852	430.7	20.68	65.76	181.99
Better Solar	1852	430.7	20.68	65.76	181.99
A2 to B2 4 candidate Pareto routes					
Shortest Time	1992	463.2	22.42	70.51	195.75
Better Solar	2037	473.7	+2.02	+1.59	+4.42
A3 to B3 9 candidate Pareto routes					
Shortest Time	1624	377.7	15.75	57.48	159.59
Better Solar 1	1627	378.4	+0.93	+0.11	+0.29
Better Solar 2	1626	378.1	+0.76	+0.07	+0.19
Better Solar 3	1693	393.7	+3.03	+2.44	+6.78
A4 to B4 4 candidate Pareto routes					
Shortest Time	1433	333.2	16.07	50.72	140.82
Better Solar	1457	338.8	+1.44	+0.85	+2.34

TABLE III: Routing Simulation 4:00 PM

Paths	TL (m)	TT (s)	EI (Wh)	EC1 (Wh)	EC2 (Wh)
A1 to B1 5 candidate Pareto routes					
Shortest Time	1852	440.9	10.13	65.35	173.65
Better Solar	1852	440.9	10.13	65.35	173.65
A2 to B2 8 candidate Pareto routes					
Shortest Time	1992	474.2	12.14	70.29	186.77
Better Solar	2037	485.1	+2.38	+1.58	+4.21
A3 to B3 4 candidate Pareto routes					
Shortest Time	1624	386.7	10.65	57.30	152.25
Better Solar	1624	386.7	10.65	57.30	152.25
A4 to B4 3 candidate Pareto routes					
Shortest Time	1433	341.2	10.21	50.51	134.34
Better Solar	1455	345.1	+1.31	+0.77	+2.07
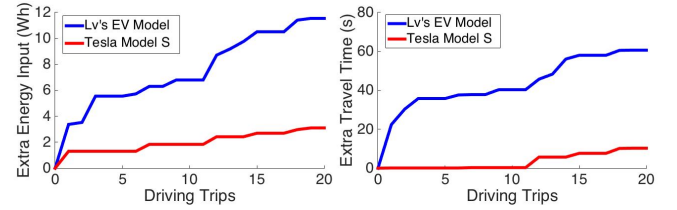
(a) Extra Solar Energy Input. (b) Extra Travel Time.

Fig. 9: One Day Driving Scenario Case 1.

could generate more candidate Pareto routes (3 for A1-B1 and 9 for A2-B2). The solar energy input EI in the first route of A2-B2 achieves 0.97 Wh more than the shortest-time path while only consuming 0.04 Wh and 0.09 Wh more energy for Lv's EV and Tesla Model S, respectively. It is a better choice for both EVs. However, the second route only has a better extra energy input for Lv's EV (6.41 > 3.31), while it does not meet the requirement for Tesla model (6.41 < 8.81). The output for A3-B3 is similar to the second route in A2-B2, which meets the need of Lv's EV but misses Tesla model's. For A4-B4, we have two better solar routes that works well for both EVs. It is mainly because that the system could find more road segments with lower/less buildings to achieve better solar energy input without significant changes in total distance.

In Table III, since the sun position becomes higher at noon, the routing conditions changed especially for A2-B2 and A3-B3. The direction of the route for A2-B2 is west-east and south-north, while for A3-B3 is west-east and north-south. The total length of solar road segments for A2-B2 decreased due to shadow rotations compared to other trips. The system could not find a proper path in A2-B2 for both Lv's EV and the Tesla model anymore, but there are two more better routes in A3-B3 compare with the results in Table II. In Table III, since solar power decreases in the afternoon there is less solar energy input (from 200/210W to 160W). We cannot find any better route for Tesla model S in all 4 cases and there are less better routes for Lv's EV. Thus driving in the morning or the

middle of the day may have more chances to achieve better solar energy input for solar-powered EVs.

As shown in Tables I, II, and III, our proposed route planning algorithm performed well in most cases, which could provide better options for solar-powered EVs with more energy input. For the cases that our algorithm fails to output a better route, the main reason is that the low panel cell efficiency can not meet the vehicle energy requirements as discussed in Section I. In addition, the route planning may also be limited by the structure of urban roads, and there may be only one or two paths from the start point to the end point. The evaluation results demonstrate that our system is robust to real road environments, and has great potential to help EV drivers achieve better on-road solar availability in the future.

2) The One-Day Driving Scenario: In the one-day driving scenario, we evaluated our route planning algorithm by using two sets of trips for two EV models through the daytime (from 9:00 a.m. to 5:00 p.m.). Each set contains 20 different pairs of start and end points. The solar radiation is determined by the time (from 160W to 210W) based on the datasets [21]. In Figures 9 and 10, we present the extra solar energy input and travel time of selected routes compared to the shortest-time paths for each case. Though there may be several candidate routes for a given trip, we only select the one which can maximize the extra solar energy input. Because it can show the worst case of extra travel time and give a better understanding of the routing algorithm performance. If there is no route with better solar energy input, we selected the shortest-time path for the trip as same as the case in the normal driving scenario.

As illustrated in Figures 9 and 10, for both Lv' EV model and Tesla Model S, the proposed algorithm is capable of providing better routes to collect extra solar energy in the

(a) Extra Solar Energy Input.
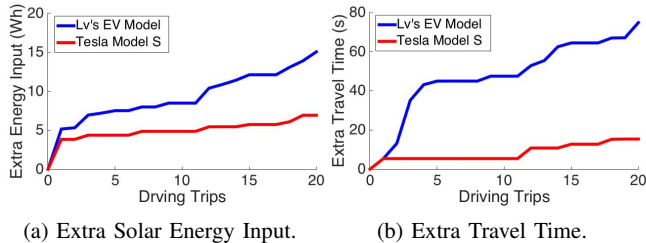
(b) Extra Travel Time.

Fig. 10: One Day Driving Scenario Case 2.

daytime. Compared to the shortest-time paths, the maximum extra travel time is from 60 seconds to 80 seconds which is acceptable. According to the results, the amount of extra solar energy input increased fast in the morning (driving trips 1 - 4). It is because that the sun kept raising across the sky, there were many shadows on roads which changed significantly in a short time. Meanwhile, the solar radiation value is relatively high (180W - 200 W), thus there is a higher probability to find routes with better solar access. At noon, the sun reached the highest position in the sky and most of the road segments were illuminated. Due to the low solar panel cell efficiency, current EV models will consume more energy than the solar input to keep moving at a normal speed. The shortest-time path would be the only option for a trip at this time which did not/hardly gain the extra solar energy input (driving trips 5 - 11). In the afternoon, the shadows were back on roads but the solar radiation is lower than the value in the morning. The algorithm can find routes with better solar access, however, they produced less solar energy than the driving trips in the morning (the curve for trips 1-4 is sharper than trips 15-20).

As we can see in Figures 9a and 10a, the Tesla Model S collected less solar energy than the Lv's EV model in one-day driving. Unlike Lv's EV model, it is more challenging to find better routes for Tesla Model S since it has a much higher energy consumption rate. In some trips, the route produced extra solar energy for Lv's model however can not meet the need of the Tesla model. In addition, we increased the physical distance between start and end points in case 2 (Figures 10). As a result, both EV models in case 2 collected higher extra solar energy inputs compared to case 1, which increased 42.7% for Lv's model (Figure 9a) and 109.7% for Tesla model (Figure 10a). Meanwhile, as shown in Figures 9b and 10b, the travel time for Lv's EV Model and Tesla Model S do not increase as significantly as the solar energy input, which are 18.6% and 36.3%, respectively. Therefore, our proposed routing algorithm could perform even better when the travel distance become longer, which offers more solar energy input with less extra travel time costs. To further prove our observations, we also consider the long-distance driving scenarios (e.g. 10 - 20 km) in the future.

VI. Discussions and Future Work

Though our proposed route planning solution achieved good performance in the evaluation, it can still be further improved by enhancing the solar access model accuracy. In this paper, we estimate the on-road shadow length by using vision-based methods on the 3D map data. The condition of illuminated and shaded road segments can be affected by roadside trees, temporary obstructions (e.g. construction areas) or clouds. For example, the shadows caused by trees will be larger during summer time due to overgrowth leaves and become sparse in the winter. Passing by clouds will change the solar radiation in a specific area and reduce the power input efficiency. However, such real-time information is not accessible via public databases, which will make the solar access estimation and route planning outputs less accurate especially for long-distance trip scenarios. Thus an on-road sensing platform that provides real-time solar access data is desirable.

On the other hand, smartphone-based sensing platforms are becoming more and more popular. Smartphones are easy accessible and affordable for everyone, which are widely used to facilitate traffic safety, together with other technologies such as autonomous driving and vehicular communications [27]. Inspired by the existing work [28], [29], we would like to seek solutions for real-time solar access measurement by leveraging crowdsensing technologies via smartphones. For example, a driver can mount the smartphone on the windshield for navigation while at the same time capturing the on-road shadow conditions using its front-facing cameras. By collecting the real-time shadow information across thousands of phones in moving vehicles, we are able to draw a comprehensive solar input map. The system can also record the traffic flow information to aid the calculation of energy input and consumption .

VII. Conclusion

In this paper, we study the route planning problem for solar-powered EVs to offer power-aware optimal routing. We define the route planning as a multi-objective optimization problem that incorporates three major factors including travel time, solar-input/access quantity and EV energy consumption. Based on the solar access model and traffic flow information, we are able to estimate the solar access on roads and run a multi-criteria search algorithm to find a set of Pareto candidate routes. We extract the most representative outputs from Pareto routes by leveraging the bisect k-means clustering algorithm. The results in both real-road experiments and simulations demonstrate that our proposed solar input model and routing algorithm are robust to real life scenarios, which have great potential to provide efficient services for solar-powered EV drivers.

References

[1] M. Lv, N. Guan, Y. Ma, D. Ji, E. Knippel, X. Liu, and W. Yi, "Speed planning for solar-powered electric vehicles," in *Proceedings of the Seventh International Conference on Future Energy Systems*. ACM, 2016, p. 6.

[2] S. Grubwinkler, T. Brunner, and M. Lienkamp, "Range prediction for evs via crowd-sourcing," in *2014 IEEE Vehicle Power and Propulsion Conference (VPPC)*. IEEE, 2014, pp. 1–6.

[3] G. Rizzo, I. Arsie, and M. Sorrentino, "Solar energy for cars: perspectives, opportunities and problems," in *Proceedings of the GTAA Meeting*, 2010, pp. 1–6.

[4] M. Sachenbacher, M. Leucker, A. Artmeier, and J. Haselmayr, "Efficient energy-optimal routing for electric vehicles." in *AAAI*, 2011.

[5] A. Artmeier, J. Haselmayr, M. Leucker, M. Sachenbacher *et al.*, "The optimal routing problem in the context of battery-powered electric vehicles," in *Workshop: CROCS at CPAIOR-10, Second International Workshop on Constraint Reasoning and Optimization for Computational Sustainability, Bologna, Italy*, 2010.

[6] S. Tang, X.-Y. Li, X. Shen, J. Zhang, G. Dai, and S. K. Das, "Cool: On coverage with solar-powered sensors," in *Distributed Computing Systems (ICDCS), 2011 31st International Conference on*. IEEE, 2011, pp. 488–496.

[7] H. C. Joksch, "The shortest route problem with constraints," *Journal of Mathematical analysis and applications*, vol. 14, no. 2, pp. 191–197, 1966.

[8] W. Dib, A. Chasse, P. Moulin, A. Sciarretta, and G. Corde, "Optimal energy management for an electric vehicle in eco-driving applications," *Control Engineering Practice*, vol. 29, pp. 299–307, 2014.

[9] M. Schneider, A. Stenger, and D. Goeke, "The electric vehicle-routing problem with time windows and recharging stations," *Transportation Science*, vol. 48, no. 4, pp. 500–520, 2014.

[10] S. Storandt, "Quick and energy-efficient routes: computing constrained shortest paths for electric vehicles," in *Proceedings of the 5th ACM SIGSPATIAL International Workshop on Computational Transportation Science*. ACM, 2012, pp. 20–25.

[11] A. Artmeier, J. Haselmayr, M. Leucker, M. Sachenbacher *et al.*, "The optimal routing problem in the context of battery-powered electric vehicles," in *Workshop: CROCS at CPAIOR-10, Second International Workshop on Constraint Reasoning and Optimization for Computational Sustainability, Bologna, Italy*, 2010.

[12] M. Baum, J. Dibbelt, T. Pajor, and D. Wagner, "Energy-optimal routes for electric vehicles," in *Proceedings of the 21st ACM SIGSPATIAL International Conference on Advances in Geographic Information Systems*. ACM, 2013, pp. 54–63.

[13] R. Dai, U. Lee, S. Hosseini, and M. Mesbahi, "Optimal path planning for solar-powered uavs based on unit quaternions," in *2012 IEEE 51st IEEE Conference on Decision and Control (CDC)*. IEEE, 2012, pp. 3104–3109.

[14] R. Dai, "Path planning of solar-powered unmanned aerial vehicles at low altitude," in *2013 IEEE 56th International Midwest Symposium on Circuits and Systems (MWSCAS)*. IEEE, 2013, pp. 693–696.

[15] S. Hosseini, R. Dai, and M. Mesbahi, "Optimal path planning and power allocation for a long endurance solar-powered uav," in *2013 American Control Conference*. IEEE, 2013, pp. 2588–2593.

[16] A. S. Challenge, "American solar challenge," 2016, http://americansolarchallenge.org/.

[17] P. A. Plonski, P. Tokekar, and V. Isler, "Energy-efficient path planning for solar-powered mobile robots," *Journal of Field Robotics*, vol. 30, no. 4, pp. 583–601, 2013.

[18] M. Sorrentino, I. Arsie, R. Di Martino, and G. Rizzo, "On the use of genetic algorithm to optimize the on-board energy management of a hybrid solar vehicle," *Oil & Gas Science and Technology–Revue de l'Institut Français du Pétrole*, vol. 65, no. 1, pp. 133–143, 2010.

[19] wikipedia, "Haversine formula," 2016, https://en.wikipedia.org/wiki/Haversine_formula.

[20] ArcGIS, "Arcgis geoinformation model," 2016, http://doc.arcgis.com/en/arcgis-online/reference/what-is-web-scene.htm.

[21] N. R. Canada, "High-resolution solar radiation datasets," 2016, http://www.nrcan.gc.ca/energy/renewable-electricity/solar-photovoltaic/18409.

[22] G. Maps, "Google maps," 2016, https://www.google.com/maps.

[23] Q. Song, P. Zilecky, M. Jakob, and J. Hrncir, "Exploring pareto routes in multi-criteria urban bicycle routing," in *17th International IEEE Conference on Intelligent Transportation Systems (ITSC)*. IEEE, 2014, pp. 1781–1787.

[24] Google, "Android environment sensors," 2016, https://developer.android.com/guide/topics/sensors/sensors_environment.html.

[25] OpenStreetMap, "Openstreetmap," 2016, https://www.openstreetmap.org/export#map=17.html.

[26] Tesla, "Model s efficiency and range," 2012, https://www.tesla.com/en_CA/blog/model-s-efficiency-and-range?redirect=no.

[27] Y. Wang, E. Yang, W. Zheng, L. Huang, H. Liu, and B. Liang, "A realistic and optimized v2v communication system for taxicabs," in *Distributed Computing Systems (ICDCS), 2016 IEEE 36th International Conference on*. IEEE, 2016, pp. 139–148.

[28] C.-W. You, M. Montes-de Oca, T. J. Bao, N. D. Lane, H. Lu, G. Cardone, L. Torresani, and A. T. Campbell, "Carsafe: a driver safety app that detects dangerous driving behavior using dual-cameras on smartphones," in *Proceedings of the 2012 ACM Conference on Ubiquitous Computing*. ACM, 2012, pp. 671–672.

[29] L. Jiang, X. Chen, and W. He, "Safecam: Analyzing intersection-related driver behaviors using multi-sensor smartphones," in *2016 IEEE International Conference on Pervasive Computing and Communications (PerCom)*. IEEE, 2016, pp. 1–9.